Kinematic condition for multicomponent lattice Boltzmann simulation

A. P. Hollis, I. Halliday, and R. Law
Materials Research Institute, Sheffield Hallam University, Howard Street, S1 1WB, United Kingdom
(Received 30 January 2007; revised manuscript received 30 May 2007; published 31 August 2007)

We present a simple, transferable, efficient, and effective algorithmic enhancement designed to improve the accuracy of all multicomponent lattice Boltzmann methods when applied to the simulation in the continuum approximation of fluid mechanics. By applying a collision parameter (kinematic viscosity) perturbation to reduce velocity gradients in the interfacial region, a kinematic condition is effectively enforced. Matters relating to a variation in the collision parameter are briefly discussed.

DOI: 10.1103/PhysRevE.76.026709 PACS number(s): 47.11.−j, 05.20.Dd, 51.10.+y

I. INTRODUCTION

Complex, multicomponent fluid flow is of widespread significance. Often, however, computational demands make its numerical calculation prohibitively expensive. The advent of multicomponent lattice Boltzmann (MCLB) simulation [1] has improved matters and a variety of flows, spanning a range of length and time scales, are currently modeled using MCLB. The simple and robust innovations reported here are relevant to all MCLB variants when applied to the continuum regime, with completely immiscible fluids. This short paper addresses the representation of an interfacial kinematic condition (KC) of mutual fluid impenetrability [2]; we shall describe in Sec. II the most appropriate MCLB model for such an application, then, in Sec. III, show how it may be simply and effectively modified explicitly to contain a KC in a manner readily transferable to other MCLBs; finally, in Sec. IV we shall present and discuss results.

Interfacial boundary conditions are treated in all MCLB as a constraint coupling the dynamics of a single component lattice Boltzmann (lB) fluid to those of an order parameter [3] or a phase field [4,5]. Thereafter, the principal MCLB methods are distinguished by the detailed way in which a fluid-fluid interface is imposed [1,4,6], with different algorithms favoring different applications. For example, in mesoscale problems where the kinematics of phase separation feature the free-energy method [6,3], based as it is upon Cahn-Hilliard theory, is the appropriate choice of MCLB. Alternatively, flows like that in Ref. [9], which are formally characterized as complex, incompressible, multicomponent flows, address the continuum fluid approximation. In the latter regime fluid-fluid interfaces are unstructured and appear as boundary conditions on $\partial\Omega_{12}$ where Ω_1 and Ω_2 are separate Navier-Stokes domains. Most MCLB variants have, at some time, been applied in this approximation but physical accuracy, efficiency, and simplicity favor a MCLB pioneered by Gunstensen *et al.* [8] and modified by Lishchuk [4] and Halliday *et al.* [10,11,5] for the continuum regime.

The MCLB method of Ref. [5] is a synthesis of the work of Lishchuk *et al.* [4], d'Ortona *et al.* [12], and Latva-Kokko and Rothman [13]. It has narrow interfaces with a thickness independent of the computational mesh resolution (but see below), an independently adjustable interfacial tension which may be large, predictable phase-field dynamics [5], and it also facilitates simulation at a low capillary and drop Reynolds number [5]. Furthermore, the MCLB method of Ref. [5] is based on the notion of dynamic, stress, boundary conditions [2] enforced over the interface between immiscible fluids [4] but neither it nor its progenitors take explicit account of any form of KC.

The present work goes some way to addressing the problems of conflicting length scales, unavoidable in MCLB, given that any practical (stable) interface must be diffuse on some characteristic, finite distance. We address this issue of interface scale and locatability implicitly, by devising a simple KC algorithm, which acts over a very limited distance on either side of a defined, subgrid interface center, which, in turn, the KC implicitly serves to define.

II. BACKGROUND

The MCLB method used in this work is that of Ref. [5]. It builds from a single component, single relaxation time lB variant designated the lattice Bhatnagar-Gross-Krook (LBGK) model [14]. LBGK has an evolution (collision, subsequent propagation) equation for a discretized single-particle momentum distribution function f_i [1] to which a source term $\phi_i(\mathbf{r})$ may be added as follows:

$$f_i(\mathbf{r}+\mathbf{c}_i,t+1)=f_i(\mathbf{r},t)-\omega[f_i(\mathbf{r},t)-f_i^{(0)}(\rho,\rho\mathbf{u})]+\phi_i(\mathbf{r}), \tag{1}$$

to impress a body force in the lattice fluid. Below we identify symbols and discuss how source term ϕ_i inserts a particular body force of limited range to produce an interfacial pressure step in the fluid. From the single-particle momentum distribution function f_i governed by Eq. (1) isothermal, hydrodynamic observables ρ and $\mathbf{u}$ emerge [1] as follows:

$$\rho(\mathbf{r},t)\equiv\sum_i f_i(\mathbf{r},t),\quad \mathbf{u}(\mathbf{r},t)\equiv\frac{1}{\rho(\mathbf{r},t)}\sum_i f_i(\mathbf{r},t)\mathbf{c}_i. \tag{2}$$

For a constant ϕ_i, Chapman-Enskog analysis [1] gives lB's characteristic, weakly compressible form of the incompressible Navier-Stokes equation, now with a constant body force. For example, the choice

$$\phi_i=t_p\frac{1}{k_2}\mathbf{F}\cdot\mathbf{c}_i \tag{3}$$

is used to insert a uniform body force in the macroscopic dynamics, which, to $o(u^2)$ [16] is

TABLE I. Link weights t_p for the D2Q9 lattice.

Link	Rest	Short	Long
$\lvert\mathbf{c}_i\rvert$	0	1	$\sqrt{2}$
t_p	4/9	1/9	1/36

$$\frac{\partial}{\partial t}\rho u_\alpha + \frac{\partial}{\partial x_\beta}\rho u_\beta u_\alpha = -\frac{\partial}{\partial x_\alpha}c_s^2\rho + \frac{\partial}{\partial x_\beta}(2\rho\nu(\omega)S_{\alpha\beta}) + \mathbf{F}_\alpha. \tag{4}$$

In the penultimate term of this equation the kinematic viscosity function $\nu(\omega)$ appears to the right of the differentiations and may be factored only for ω=constant; this is akin to the situation in physical fluids [2]. We shall return to this point. For the D2Q9 model $\nu(\omega)\equiv\frac{1}{6}(\frac{2}{\omega}-1)$. In Eq. (4) $S_{\alpha\beta}$ is the strain rate tensor; in Eq. (3) the link weights t_p are defined in Table I. The microscopic source term ϕ_i of Eq. (1), and the macroscopic force are related by

$$\mathbf{F} = k_2\sum_i \phi_i\mathbf{c}_i. \tag{5}$$

The value of constant $k_2\delta_{\alpha\beta}\equiv\Sigma_i t_p c_{i\alpha}c_{i\beta}$ used in Eqs. (3) and (5) is lattice dependent; $k_2=1/3$ for the D2Q9 model.

For present purposes, the body force needs to contain spatial variation [10] which necessitates spatial variation in $\phi_i(\mathbf{r})$. This obstructs the emergence of Eq. (4). A solution to this problem, given by Guo *et al.*, requires (i) a more complicated relationship between $\mathbf{F}(\mathbf{r})$ and $\phi_i(\mathbf{r})$ than that of Eq. (5) and (ii) a redefinition of $\mathbf{u}$. Before stating a modified relationship in Eqs. (11) and (12) below, we consider the form of fluid interface force, which ϕ_i should generate, and where this force should be applied.

Fluid-fluid interface dynamics are applied in regions of the lattice where two immiscible fluids interact. The two fluids concerned we designate red and blue. The momentum distribution function f_i is now specified for red and blue fluids individually as follows:

$$f_i(\mathbf{r},t) = R_i(\mathbf{r},t) + B_i(\mathbf{r},t), \tag{6}$$

with the nodal density now also defined for red and blue fluids individually as follows:

$$R(\mathbf{r},t)\equiv\sum_i R_i(\mathbf{r},t), \quad B(\mathbf{r},t)\equiv\sum_i B_i(\mathbf{r},t). \tag{7}$$

Note, Eqs. (2) remain valid; the velocity of a single *sum* lattice fluid is still defined by the second of Eqs. (2). As red and blue fluids mix under the lB propagation step they form a single mixture or sum fluid described by Eq. (1), with the interface dynamics (but not its kinematics) captured in the microscopic source term ϕ. The interface force (capturing the effects of interfacial tension) is applied in mixed lattice regions to the sum fluid. To identify such regions our MCLB uses a scalar phase field $\rho^N(\mathbf{r})$ as follows:

$$\rho^N(\mathbf{r},t)\equiv\left(\frac{R(\mathbf{r},t)-B(\mathbf{r},t)}{R(\mathbf{r},t)+B(\mathbf{r},t)}\right), \quad -1\leqslant\rho^N(\mathbf{r})\leqslant 1, \tag{8}$$

inverting which definition we obtain $R(\mathbf{r},t)=\frac{1}{2}\rho(\mathbf{r},t)[1+\rho^N(\mathbf{r},t)]$ and $B(\mathbf{r},t)=\frac{1}{2}\rho(\mathbf{r},t)[1-\rho^N(\mathbf{r},t)]$. The mixture is then segregated in a process, which influences the physical accuracy of the model [5], as discussed below.

The surface tension inducing interface force $\mathbf{F}(\mathbf{r})$ is defined in terms of the gradient of $\rho^N(\mathbf{r})$. To achieve a cross-interfacial pressure step proportional only to αK, the local curvature in the ρ^N field use a fluid body force as follows:

$$\mathbf{F}(\mathbf{r})\equiv-\tfrac{1}{2}\alpha K\boldsymbol{\nabla}\rho^N, \tag{9}$$

with α a surface tension parameter [4,5]; note that curvature

$$K = n_x n_y\left(\frac{\partial}{\partial y}n_x + \frac{\partial}{\partial x}n_y\right) - n_x^2\frac{\partial}{\partial y}n_y - n_y^2\frac{\partial}{\partial x}n_x, \tag{10}$$

where $\hat{\mathbf{n}}\equiv-\frac{\nabla\rho^N}{|\nabla\rho^N|}$ [10]. Our interface algorithm is apparently based on varying local force in the sum fluid, to eliminate curvature in the phase field. This device represents interface dynamics (stress conditions) [4]. But the extent to which the kinematic condition of mutual impenetrability is implicit is unclear; forcing the single, sum fluid means the combined momentum of the mixture of fluids is continuous across an interfacial region but separate red and blue fluid velocities may not be easily defined.

Guo *et al.* have treated spatially varying body forces following Verberg and Ladd [15]; a spatially varying source term $\phi_i(\mathbf{r})$ is defined in terms of the target macroscopic force $\mathbf{F}(\mathbf{r})$ [11] as follows:

$$\phi_i(\mathbf{r})\equiv t_p\left(1-\frac{\omega}{2}\right)[3(\mathbf{c}_i-\mathbf{u}^*)+9(\mathbf{c}_i\cdot\mathbf{u}^*)\mathbf{c}_i]\cdot\mathbf{F}(\mathbf{r}), \tag{11}$$

where our MCLB velocity is redefined as follows:

$$\mathbf{u}^*\equiv\frac{1}{\rho}\left(\sum_i f_i\mathbf{c}_i + (1-f)\frac{1}{2}\mathbf{F}(\mathbf{r})\right), \quad f=\frac{1}{2}, \tag{12}$$

and $\mathbf{F}(\mathbf{r})$ is given by Eq. (9). Note that the quantity f introduced above is discussed shortly. Navier-Stokes equation (4) now accurately acquires position-dependent body forcing as follows:

$$\frac{\partial}{\partial t}\rho u_\alpha^* + \frac{\partial}{\partial x_\beta}\rho u_\beta^* u_\alpha^* = -\frac{\partial}{\partial x_\alpha}(c_s^2\rho) + \nu(\omega)\frac{\partial}{\partial x_\beta}(2\rho S_{\alpha\beta}^*) + F_\alpha(\mathbf{r}), \tag{13}$$

and an exact continuity equation. In fact, all other MCLB models impose an interface through a generalized force, using a microscopic source ϕ_i. For example, the Oxford MCLB mesoscale model [6] imposes a structured interface appropriate to this length scale by adjusting the pressure tensor of their MCLB model [3,6].

By introducing the quantity f in Eq. (12), it [Eq. (12)] describes both Guo's model, identified by the source term equation (11), the macroscopic momentum equation (13),

and $f=1/2$, and what we term the standard model, identified by the source term equation (9), the macroscopic momentum equation (4), and $f=1$.

With the convention that a postcollision, prepropagation quantity is indicated by a dagger superscript, Eq. (1) may be recast as follows:

$$f_i^{\dagger}(\mathbf{r},t) = f_i(\mathbf{r},t) - \omega[f_i(\mathbf{r},t) - f_i^{(0)}(\rho,\rho\mathbf{u})] + \phi_i(\mathbf{r}). \quad (14)$$

Postcollision, postsegregation (recolored) quantities are indicated by the use of a double dagger superscript. Accordingly, we write Latva-Kokko and Rothman's form of D'Ortona's segregation [13,12] as follows:

$$R_i^{\dagger\dagger} = \frac{R}{R+B} f_i^{\dagger} + \beta \frac{RB}{R+B} t_p \cos(\theta_f - \theta_i)\mathbf{c}_i, \quad (15)$$

in which θ_f (θ_i) is the angle of the color field $\nabla\rho^N$ (link) and $R_i^{\dagger\dagger}$ denotes the postcollision, postsegregation value of the red fluid's momentum density associated with link i. Note that, for stable continuum interfaces segregation parameter, $\beta < 0.72$ [5].

Equation (66) of Ref. [5] describes the dynamics for the phase-field scalar ρ^N for any MCLB scheme based upon the segregation method outlined above which uses a LBGK model and either the standard method of applying a body force, or Guo's more accurate method,

$$\partial_t \rho\rho^N + \nabla\cdot(\rho\rho^N\mathbf{u}^*) = -f\nabla\cdot(\rho^N\mathbf{F}) + \tfrac{1}{2}c_s^2\nabla\cdot(\rho^N\nabla\rho). \quad (16)$$

In fact, the order parameter employed in the Oxford MCLB mesoscale model [6] to define the component (or, more accurately in this case, phase) obeys a broadly similar dynamical equation.

For the standard model [with a direct velocity $f=1$ in Eq. (12)] it is possible to obtain for the dynamics of the phase field [5],

$$\frac{d}{dt}\rho^N = -\frac{1}{2\rho}\mathbf{F}\cdot\nabla\rho^N, \quad (17)$$

which equation clearly deviates significantly from the correct form required for a continuum fluid, namely (see Sec. III),

$$\frac{d\rho^N}{dt} = 0. \quad (18)$$

However, with Guo's more accurate representation of body forces [with an indirect velocity, $f=1/2$ in Eq. (12)], the phase-field dynamics takes a more amenable form. By using Eqs. (63), (67), (68), and (83) of Ref. [5] directly, it is possible to obtain

$$\frac{d}{dt}\rho^N = \frac{1}{2\rho}\nabla\cdot(c_s^2\rho^N\nabla\rho - \rho^N\mathbf{F}) + \frac{1}{2\rho}\nabla\cdot\Delta, \quad (19)$$

where the components of vector Δ are given by

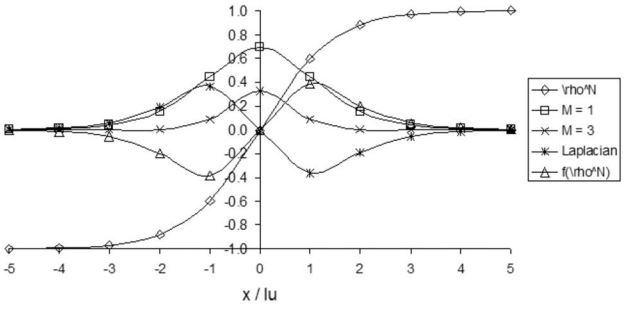

FIG. 1. Variation of quantities across the interfacial region. In the figure key, $M=1,3$ identifies the variation of $\delta\omega/K$ in Eq. (22) for $M=1,3$; f denotes $f(\rho^N)$ in Eq. (26). The interface, defined by $\rho^N=0$, is centered on $x=0$ locally.

$$\Delta_\alpha = \partial_\beta(\rho\rho^N u_\alpha^* u_\beta^*) + \frac{1}{2}\partial_\beta(\rho^N[u_\alpha^* F_\beta + u_\beta^* F_\alpha]) + 2\left(1-\frac{1}{\omega}\right)c_s^2\partial_\beta(\rho^N S_{\alpha\beta}), \quad (20)$$

in which the senior term on the right-hand side, the second, contains phase-field gradients through the interface force components F_α.

In an interfacial region, the principal contribution to any local pressure gradient may well arise from the interfacial body force $\mathbf{F}$ which, recall, generates the interfacial pressure step in our model. It is then possible to approximate $\mathbf{F} \approx c_s^2\nabla(\rho)$ and, accordingly, Eq. (19) approaches much more closely the target form, given in Eq. (18), due to a much smaller right-hand side, which is second order in gradient quantities as follows:

$$\frac{d\rho^N}{dt} = \frac{1}{2\rho}c_s^2\partial_\alpha(\rho^N\partial_\alpha[\delta\rho]) + \frac{1}{2\rho}\partial_\alpha\partial_\beta(\rho^N[u_\alpha^* F_\beta + u_\beta^* F_\alpha]). \quad (21)$$

Note that the quantity $\delta\rho$ excludes the density fluctuation due to the interface force, i.e., due to interfacial tension.

III. KINEMATIC CONDITION

In a continuum fluid, the interface is subject to a kinematic condition (KC), which effectively requires that it move at the same speed as the local fluids. For a point in the interface, identified by a chosen value of ρ^N, to advect in flow $\frac{d\rho^N}{dt}=0$. It follows from Eqs. (19) or (21) that the interface is accelerated relative to the local fluid by an amount determined by pressure and phase-field gradients. The remainder of this paper is concerned with a remedy to this absence of an intrinsic KC, portable into other MCLB methods and rather more in accord with the spirit of lB simulation than earlier attempts based upon a momentum conserving process of averaging the separated fluids' velocity in the interfacial region [10]. The latter method is of very limited value; it is reliant upon arbitrary, computationally expensive site selection criteria and it compromises interface resolution.

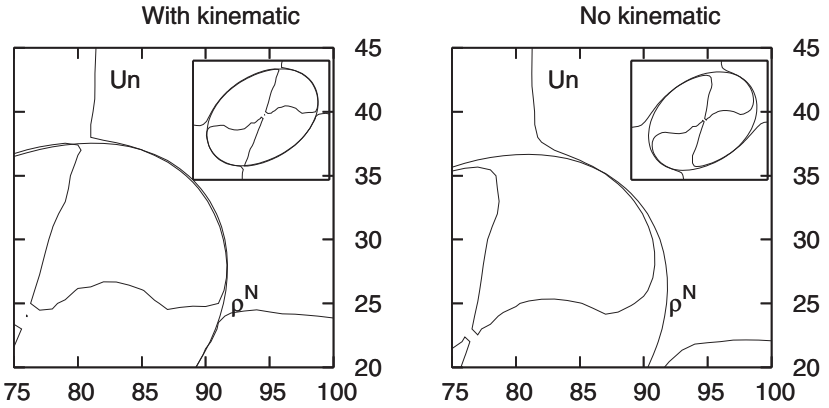

FIG. 2. Normal velocity $u_n=0$ contour superimposed over $\rho^N=0$ contour of a sheared drop at steady state, with (left) and without (right) the kinematic condition of Eq. (22) in effect. Note the departure of the $\rho^N=0$ and $u_n=0$ contours in the "polar" and "equatorial" regions in the figure on the right.

Consider a static, spherical red drop, nominal radius $r_0=50$, suspended in a blue fluid; such a drop is described by a phase-field variation $\rho^N=\tanh[\beta(r-r_0)]$ for $\beta<0.7$ [5]. Figure 1 shows the variation of the phase field ρ^N in the radial direction, across the interface (diamonds); note, abscissa $x=0$ is the interface center. Variation of the Laplacian of the ρ^N field [which, broadly determines the variation of the second term in the right-hand side of Eq. (21) and the divergence of **F**, which is the principal contribution to the right-hand side of Eq. (19)] is plotted using asterisks. On contour $\rho^N=0$ (at $x=0$) of our particular MCLB's interface, a KC is approximately satisfied in both models, with the Guo model [$f=1/2$, Eq. (21)] much the superior. In general, however, the gradients of ρ^N vary and the interface is accelerated most rapidly for positions $|x|\leqslant 1$, corresponding to $|\rho^N|<0.5$. This is true for all interface radii or curvatures. The region $|\rho^N|<0.5$ suggests itself as the interfacial zone onto which algorithmic extensions designed to promote a KC should be concentrated.

To promote correlated motion between the internal (red) and external (blue) fluids at the boundary we seek to eliminate fluid shear in a thin shell $|\rho^N|<0.5$, which, from Fig. 1, is about three lattice units thick. This is accomplished by

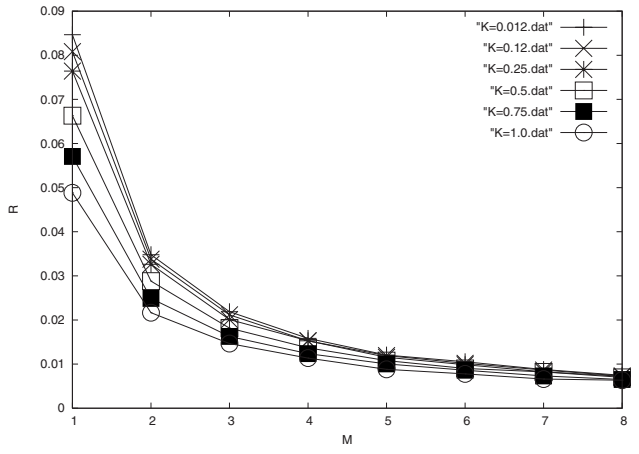

FIG. 3. Absolute value of R, the steady-state residual of the interface normal velocity u_n (ordinate), defined in Eq. (27), plotted against M (abscissa) for different values of K; M, K as in collision parameter perturbation equation (22) for the simulation defined in the first paragraph of Sec. IV.

increasing the local sum fluid viscosity using a collision parameter perturbation as follows:

$$\delta\omega = -K(1-\rho^{N2})^M, \quad |\rho^N| \leqslant 0.5, \quad K,M>0, \tag{22}$$

corresponding in D2Q9 to a local viscosity increase as follows:

$$\delta\nu = \frac{1}{3}\frac{K}{\omega^2}(1-\rho^{N2})^M = \frac{1}{3}\frac{K\beta^M}{\omega^2}|\nabla\rho^N|^M, \tag{23}$$

in which we have used a property of interfaces generated by the formulaic segregation of Eq. (15), after D'Ortona [12] and Latva-Kokko *et al.* [13], derived in Ref. [5], namely,

$$|\nabla\rho^N| = \beta(1-\rho^{N2}). \tag{24}$$

The requirement $\nu>0$; $0<\omega<2$ constrains the choice of K; Fig. 1 plots the variation of $\delta\omega$ for $K=1$, $M=1$ (open squares) and $K=1$, $M=3$ (triangles); for the case of $M=3$ perturbation $\delta\omega$ is significant only for $|\rho^N|>0.5$, which advantageously limits any penalty on resolution in the interfacial region; with $M=3$ sites at $x=\pm 2$ are unaffected, further adjustment of $M:M>3$, $M<10$ does not change this observation but degrades stability. Clearly, the extension in Eq. (23) generalizes readily to all other MCLB variants [3,7], and is easy to apply in three dimensions (3D).

When considering incompressible liquids, one traditionally factorizes $\nu(\omega)$ in Eq. (4), whereupon any spatial variation in the latter will generate additional force terms. This encourages the view of an incompressible, fluid, interfacial region of variable viscosity, subject to a compensatory forcing, which effectively restores a KC. It is worth remarking that a variation in kinematic viscosity ν may characterize a particular problem, for example, when modeling spatial variation in fluid temperature within the Boussinesq approximation. Any such variation should be modeled with ν, positioned as in Eq. (4), behind the first spatial differentiation in the second term in the right-hand side of Eq. (4).

Consider the case of Guo's (adjusted velocity) model. Factorization of $\nu(\omega)$ exposes an effective, shear-rate-dependent forcing in the right-hand side of the lattice Navier-Stokes equation (13) as follows:

$$F'_\alpha = 2\rho S^*_{\alpha\beta}\frac{\partial}{\partial x_\beta}\nu(\omega) = -\frac{2}{3}\frac{\rho}{\omega^2}S^*_{\alpha\beta}\frac{\partial}{\partial x_\beta}\delta\omega, \tag{25}$$

in which the last equality uses a substitution for $\nu(\omega)$ for the case of a D2Q9 model. Here strain rate $S^*_{\alpha\beta}$ is based upon gradients in the corrected velocity of Eq. (12).

With our proposed ω variation of Eq. (22) we obtain from Eq. (25), by straightforward use of Eqs. (23) and (24),

$$F'_\alpha = -\frac{4\rho\beta}{3\omega^2}KMf(\rho^N)S^*_{\alpha\beta}f'_\beta, \quad f(\rho^N) \equiv \rho^N(1-\rho^{N2}). \tag{26}$$

It is not surprising to find an equivalence between an interfacial viscosity perturbation, suggested in Eq. (23) and an effective shear-rate-dependent force. The factor $f(\rho^N)$ defined above, varies across the interfacial region as illustrated in Fig. 1.

IV. RESULTS AND DISCUSSION

Figures 2 and 3 all derive from data obtained from drops of initial radius 15 lattice units, with surface tension parameter $\alpha = 7.0\times10^{-3}$. For the the data of Fig. 2 the drop was exposed to an unperturbed shear rate 1.0×10^{-4} in lattice units, on a lattice of size 150×50 lattice units; the unperturbed collision parameter $\omega=1.0$ and the perturbation $\delta\omega$ [Eq. 2] was characterized by $K=0.5$, $M=2$. For Fig. 3, the same lattice with rest boundaries was used, with a range of viscosity perturbations (see the figure key and caption).

Consider a neutrally buoyant (red) drop embedded in a symmetrical sheared (blue) fluid of identical kinematic viscosity. At the steady state, in the rest frame of the drop interface deformation ceases and the normal component of fluid velocity, u_n, vanishes (this is untrue of the corresponding tangential component, which is nonzero in general). On noting that the chosen interface center, the contour $\rho^N=0$ cannot intersect any lattice node, we suggest that the best illustration of the subgrid nature of the KC and the benefits attending its use is the correlation between the contour $\rho^N=0$ and the contour $u_n=0$. Compare now the results in Fig. 2. On the right of this figure is shown details of the flow in the region of the drop pole; the $u_n=0$ contour is superposed over the (closed) contour ρ^N, for a drop without a KC inducing perturbation in force; the figure inset shows the whole drop. On the left of Fig. 2 is the corresponding simulation with a KC, characterized by $K=1$, $M=3$ applied. In the latter, the $u_n=0$ contour is located much closer to the center of the interface, especially in the polar region, where u_t, the component of fluid velocity tangent to the $\rho^N=0$, was also much smaller.

Briefly consider the effective, shear dependent force $\mathbf{F}'$ of Eq. (25) at the "North Pole" of the drop depicted in Fig. 2. The shear rate at the drop North Pole is dominated by a contribution $\frac{\partial v_x}{\partial x}>0$; this, and the variation of the the factor $f(\rho^N)$ imply $F'_x<0$ $(F'_x>0)$ for the blue (red) side of the interface, in accord with a reduction of the local shear gradient when $\rho^N=0$.

In Fig. 3 we consider the correlation of the zero of normal velocity with the $\rho^N=0$ contour. The ordinate corresponds to a steady-state residual of the modulus of the normal velocity as follows:

$$R = \sum_{\rho^N=0} |u_n|, \tag{27}$$

the abscissa to the value of parameter M in Eq. (22). Branches of the plot with increasing ordinal intercept correspond to amplitude parameter

$$K = 1.00, 0.75, 0.50, 0.25, 0.12, 0.012$$

in Eq. (22). Our simulations show that the correlation improve at a diminishing rate as M increases; while our simulations were stable, as M increases, larger shear rates may cause instability.

The segregation method outlined in this paper together with a kinematic condition facilitate robust MCLB simulations in the continuum approximation with advantages of increased efficiency, negligible interfacial microcurrent activity, and drop pinning [13,5] (facilitating low capillary and drop Reynolds number [5] applications), improved representation of continuum hydrodynamic boundary conditions (Fig. 2) and, not least, simplicity. Moreover, the simple rule expressed in Eq. (22) transplants into other MCLB methods [6,7] directly, to facilitate their application to the continuum regime.

[1] S. Succi, *The Lattice Boltzmann Equation for Fluid Dynamics and Beyond* (Clarendon Press, Oxford, 2001).

[2] L. Landau and E. M. Lifshitz, *Fluid Mechanics*, 2nd ed., (Butterworth-Heinemann, Oxford, 1987).

[3] M. R. Swift, E. Orlandini, W. R. Osborn, and J. M. Yeomans, Phys. Rev. E **54**, 5041 (1996).

[4] S. V. Lishchuk, C. M. Care, and I. Halliday, Phys. Rev. E **67**, 036701 (2003).

[5] I. Halliday, A. P. Hollis, and C. M. Care, preceding paper, Phys. Rev. E **76**, 026708 (2007).

[6] M. R. Swift, W. R. Osborn, and J. M. Yeomans, Phys. Rev. Lett. **75**, 830 (1995).

[7] X. W. Shan and H. D. Chen, Phys. Rev. E **49**, 2941 (1994).

[8] A. K. Gunstensen, D. H. Rothman, S. Zaleski, and G. Zanetti, Phys. Rev. A **43**, 4320 (1991).

[9] M. M. Dupin, I. Halliday, and C. M. Care, Phys. Rev. E **73**, 055701(R) (2006).

[10] I. Halliday, R. Law, C. M. Care, and A. Hollis, Phys. Rev. E **73**, 056708 (2006).

[11] Z. Guo, C. Zheng, and B. Shi, Phys. Rev. E **65**, 046308 (2002).

[12] U. D'Ortona, D. Salin, M. Cieplak, R. B. Rybka, and J. R.

Banavar, Phys. Rev. E **51**, 3718 (1995).
[13] M. Latva-Kokko and D. H. Rothman, Phys. Rev. E **71**, 056702 (2005).
[14] Y. H. Qian, D. d'Humieres, and P. Lallemand, Europhys. Lett. **17**, 479 (1992).
[15] A. J. C. Ladd and R. Verberg, J. Stat. Phys. **104**, 1191 (2001).
[16] S. Hou, Q. Zou, S. Chen, G. Doolen, and A. C. Cogley, J. Comput. Phys. **118**, 329 (1995).